Biophysical Chemistry 180–181 (2013) 110–118

Contents lists available at SciVerse ScienceDirect

Biophysical Chemistry

journal homepage: http://www.elsevier.com/locate/biophyschem

Propensities for loop structures of RNA & DNA backbones

Antonella Paladino [a], Ronen Zangi [a,b,*]

[a] Department of Organic Chemistry I, University of the Basque Country UPV/EHU, Avenida de Tolosa 72, 20018 San Sebastian, Spain
[b] IKERBASQUE, Basque Foundation for Science, 48011 Bilbao, Spain

HIGHLIGHTS

- Loop motifs are abundant in RNA but not in DNA structures.
- There are differences in the backbone dihedrals between RNA and DNA.
- We study computationally the relation between these dihedrals and loop structures.
- However, we did not find strong correlations.
- The preference for loops is found to be due to the ribose 2′-hydroxyls in RNA.

GRAPHICAL ABSTRACT

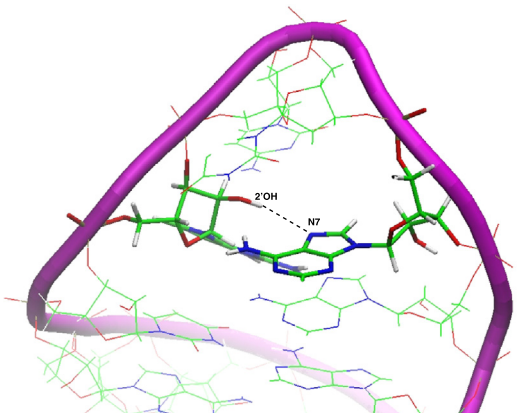

ARTICLE INFO

Article history:
Received 10 June 2013
Received in revised form 10 July 2013
Accepted 10 July 2013
Available online 20 July 2013

Keywords:
Ribose versus deoxyribose
Hairpin motif
Backbone dihedral
Sugar puckering
Molecular dynamics
Replica-exchange simulation

ABSTRACT

RNA oligonucleotides exhibit a large tendency to bend and form a loop conformation which is a major motif contributing to their complex three-dimensional structure. This is in contrast to DNA molecules that predominantly form the double-helix structure. In this paper we investigate by molecular dynamics simulation, as well as, by its combination with the replica-exchange method, the propensity of RNA chains containing the GCUAA pentaloop to form spontaneously a hairpin conformation. The results were then compared with those of analogous hybrid oligonucleotides in which the ribose groups in the loop-region were substituted by deoxyriboses. We find that the RNA oligomers exhibit a marginal excess stability to form loop structures. The equilibrium constant for opening the loop to an extended conformation is twice as large in the hybrid than it is in the RNA chain. Analyses of the hydrogen bonds indicate that the excess stability for forming a hairpin is a result of hydrogen bonds the 2′-hydroxyls in the loop region form with other groups in the loop. Of these hydrogen bonds, the most important is the hydrogen bond donated from the 2′-OH at the first position of the loop to N7 of adenine at the forth position. RNA and DNA backbones are characterized by different backbone dihedral angles and sugar puckering that can potentially facilitate or hamper the hydrogen bonds involving the 2′-OH. Nevertheless, the sugar puckerings of all the pentaloop nucleotides were not significantly different between the two chains displaying the C3′-endo conformation characteristic to the A-form double helix. All of the other backbone dihedrals also did not show any considerable difference in the loop-region except of the δ-dihedral. In this case, the RNA loop exhibited bimodal distributions corresponding to, both, the RNA and DNA backbones, whereas the loop of the hybrid chain behaved mostly as that of a DNA backbone. Thus, it is possible that the behavior of the

* Corresponding author at: Department of Organic Chemistry I, University of the Basque Country UPV/EHU, Avenida de Tolosa 72, 20018, San Sebastian, Spain. Tel.: +34 943018112.
E-mail address: r.zangi@ikerbasque.org (R. Zangi).

0301-4622/$ – see front matter
http://dx.doi.org/10.1016/j.bpc.2013.07.003

δ-dihedrals in the loop-region of the RNA adopts conformations that facilitate the intra-nucleotide hydrogen bondings of the 2′-hydroxyls, and consequently renders loop structures in RNA more stable.

1. Introduction

In analogy to proteins, RNA molecules are involved in many functions in the cell, from their role in encoding genetic information to catalyzing biochemical reactions. This diversity in tasks is manifested by myriad of folded conformations that are determined by the sequence of the molecule's building blocks. For proteins these building blocks are the amino acids whereas for RNA they are the four nucleotides G, C, A, and U. Thus, chemically, proteins and RNA are very different. RNA does, however, resemble DNA. The major difference between the two is that in RNA the backbone sugars are riboses whereas in DNA there are deoxyriboses. That means, in RNA there is a hydroxyl instead of a hydrogen at position 2′ of the sugar's ring. Another difference in the chemical structure is that instead of uracil bases in RNA, thymine (which is 5-methyluracil) is utilized in DNA.

Albeit the similarities between RNA and DNA, from a structural point of view, the two molecules behave differently. DNA adopts a repetitive structure of a B-form double-helix formed by two different complementary DNA strands. In contrast, RNA is normally single-stranded and its three-dimensional structure is complex with different structural motifs. An important structural element in RNA is the A-form double-helix which is predominantly found in the stems. Structurally, the A-form double-helix is characterized by a deep and narrow major groove and a shallow and wide minor groove compared with the corresponding grooves in the B-form. Although, RNA is a single-stranded chain, the base-pairings forming the double-helix are possible due to the existence of a terminal (or hairpin) loop (hereafter, loop) in which the chain folds back on itself. Loops of different nucleotide lengths are found in RNA but tetraloops are the most abundant [1,2]. Other structural elements of RNA are internal loops (due to mismatched bases), bulges (excess of residues on one side of the duplex) and triple-base-interactions.

The difference between uracil and thymine in the sequence of RNA and DNA is not large and is not likely to account for the structural differences observed between the two oligonucleotides. As far as the different conformations of the double-helix are concerned, these are likely to be the result of the presence or absence of the 2′-hydroxyls. This argument is supported by an X-ray study showing that the-introduction of a single 2′-hydroxyl group in the backbone of B-DNA can convert it to A-DNA [3]. However, are the other structural motifs characteristic to RNA, but not present in DNA, stabilized by these ribose hydroxyls or are they merely results of the sequence of the bases? By definition, internal loops and bulges necessitate defects in the Watson-Crick and wobble base-pairings, therefore, there are indeed some sequence requirements. Nevertheless, experiments using gel electrophoresis and fluorescence resonance energy transfer demonstrated that the 2′-hydroxyls stabilize the folded conformation of a kink-turn RNA [4]. It was found that the stability does not originate uniformly from all the 2′-OH present in the region of the loop but was strongly dependent on the position of the ribose hydroxyl. More specifically, the most important interaction involved a hydrogen bond donation from the 2′-OH at the first position of the loop to N1 of adenine at the kink.

It is well documented that the ribose hydroxyls stabilize many tertiary structures, such as the ribose-zipper and the A-minor motifs [5–10], and were found to be directly involved in many processes [11–20]. Can the 2′-hydroxyls also facilitate the oligonucleotide chain to make a U-turn, i.e., form a hairpin? The fact that sequences of hairpin loops are not random combinations of the four RNA bases, and some sequence patterns are more likely to adopt a loop structure than other sequences, implies that the identity of the bases in the loop is important. Nevertheless, NMR [21] and X-ray [22] studies of hairpins containing the stable UUCG tetraloop, found that the 2′-hydroxyls in the loop region form intra-nucleotide hydrogen bonds. Furthermore, a DNA analog of this tetraloop exhibited more flexibility, less structure, and substantial loss in its catalytic activity [23]. In a different study it was found that the melting temperature of this tetraloop is 8 °C lower than that of the corresponding RNA [24]. Later, it was shown that also in this case the effect of the ribose to deoxyribose substitutions is position dependent [25,26]. Again, the substitution of the first position in the tetraloop exhibits the largest destabilization. By using restraint dynamics to stabilize the conformation in the folded or extended state, as well as, by selecting a possible pathway for the unfolding process, it was shown that the thermodynamic and kinetic stability of a GCUAA pentaloop motif in RNA is enhanced by the 2′-hydroxyl groups in the loop region [27]. Also in this case, the formation of a hydrogen bond between the 2′-OH at the first position of the loop and the adenine base at the forth position was found to be the dominant factor stabilizing the hairpin.

In contrast to the results from the UUCG and GCUAA sequences, studies on a hairpin that contains the GCAA tetraloop indicated that the ribose to deoxyribose substitution of the first base of this loop resulted in a negligible change in the melting temperature of the hairpin [28]. It was therefore concluded that the 2′-OH at the first position of this tetraloop does not affect the thermodynamic stability of the hairpin. The different behaviors of the GCAA loop suggest that the contribution of the 2′-hydroxyls to the stability of a loop might be sequence dependent.

As mentioned above, oligonucleotides with ribose backbone (i.e., RNA) primarily adopt the A-form double-helix conformation whereas those with dexoyribose backbone (DNA) adopt the B-form conformation. One of the structural differences between these two helix forms is the conformation of the ring of the sugar; in the B-form helix the sugars pucker in the C2′-endo state and in the A-form conformation the sugars pucker in the C3′-endo state. Recently, it was shown that the ribose 2′-hydroxyls stabilize the three dimensional structure of a human telomeric RNA (TERRA) quadruplex [9]. In this case it was found that the C3′-endo sugar conformation enhances the hydrogen bonds involving the 2′-OH and therefore, leads to a greater stability of the RNA tertiary structure. Does the conformation of the C3′-endo state allow the 2′-hydroxyls to form hydrogen bonds with stronger interaction energies, and thereby augment the thermodynamic stability, also in the case of loop structures?

Computer simulations of DNA and RNA systems have been increasingly popular in recent years [29–32]. For the latter, the most attractive model system has been probably the hairpin motif because it offers the ability to restrict the system to a small size. These studies were typically aimed at investigating the folding, stability and dynamics of the hairpin [33–41]. In this paper we perform molecular dynamics simulations of hairpins with the GCUAA pentaloop. The system is dynamically evolved without the influence of any restraints or non-covalently bonded constraints to ensure that the oligonucleotide is not subject to external forces that can somehow modify its conformations. In addition we also performed replica-exchange simulations at different temperatures to observe spontaneous opening and closing events of the hairpin. We find that the GCUAA pentaloop displays a larger thermodynamic stability with a RNA backbone (thus, with ribose sugars) relative to a corresponding chimeric oligomer in which the loop-region has a DNA backbone (deoxyribose sugars). The larger tendency of a RNA backbone to form loop structures is a result of hydrogen bonds the 2′-hydroxyls form in the loop-region. Structural analyses indicate that the sugar

puckerings and many of the backbone dihedrals in the loop-region show similar behavior in both oligonucleotides. However, the δ-dihedrals of the pentaloop exhibit different distributions and it well may be that the behavior observed in the loop of the RNA facilitates the formation of the 2′-OH hydrogen bonds.

2. Methods

We are interested in understanding the effect of the ribose 2′-OH on the conformation of the backbone and to correlate the effect to the change in the stability of loop structures. Our model system contains the GCUAA pentaloop structure which belongs to the central region of the human R/G stem-loop pre-mRNA (PDB access code 1YSV). In the untruncated model, a 27-nucleotide length hairpin was considered, the same as that studied experimentally [42]. Of these 27 nucleotides, 22 form eleven base-pairs defining the stem, whereas, the middle 5 unpaired nucleotides define the loop. However, in order to observe (statistically significant) spontaneous transitions between hairpin (folded) and extended (unfolded) states, we also truncated the experimental hairpin at the stem, symmetrically from both the 5′ and 3′ ends, to an 11-mer oligonucleotide. For both systems, we simulated an all-ribose RNA sequence, as well as, a chimeric oligonucleotide in which the riboses of the pentaloop, together with two neighboring riboses on each side of the pentaloop, are replaced by deoxyriboses (see Fig. 1). Thus, the latter is a hybrid of RNA and DNA backbones (hereafter referred to as 'hybrid') that contains seven deoxyriboses at the center of the molecule. Two out of the seven nucleotides that were modified from ribose to deoxyribose are uracils. In this case, we also changed the uracil base to thymine in the hybrid oligonucleotides. Note that the stem of the truncated 11-mer oligonucleotide is closing with a G:U/T wobble base-pair. The starting conformations for all simulations were based on the first conformer, out of the thirteen, deposited in the Protein Data Bank.

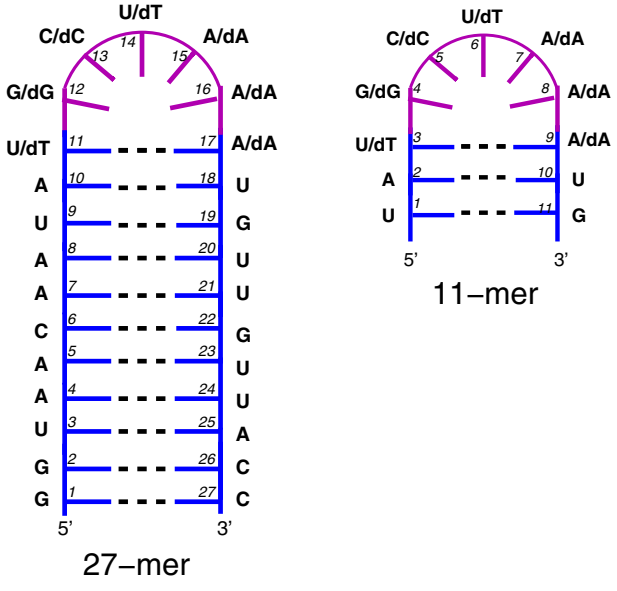

Fig. 1. The model systems that were simulated in this study. The 11-mer nucleotides are truncated version of the full-length 27-mers. The pentaloop is depicted in magenta. The seven ribose nucleotides of the RNA that were transformed in the hybrid chains to their deoxyribose counterparts are indicated. These nucleotides include the pentaloop and one nucleotide on each side of the loop. (For interpretation of the references to color in this figure legend, the reader is referred to the web version of this article.)

2.1. The 27-mer model

To neutralize the negative charge of the twenty-six phosphate groups of the oligomer, a total of twenty-six sodium cations were added at random positions to the simulation box. The size of the rectangular simulation box was determined by imposing a minimum distance of 1.0 nm between the molecule and the box walls. Then, this simulation box was filled with 8847 water molecules for both the RNA and hybrid systems.

2.2. The 11-mer model

The RNA and hybrid models were obtained by deleting the first and last eight base-pairs of the stem of the 27-mer oligonucleotide. The dimensions of the rectangular simulation box were obtained by imposing a minimum distance of 1.4 nm from the oligonucleotides atoms to the box walls, and then the system was solvated with 3579 and 3617 water molecules for the RNA and hybrid oligomers, respectively. Ten sodium cations were placed randomly in each of the simulation boxes to neutralize the systems.

For both the 27-mer and 11-mer models, the system was first energy minimized using the steepest-descent method, followed by 4 ns dynamic simulation at 300 K in which the positions of the system heavy atoms were restrained by a harmonic potential with a force constant of 1000 kJ/(mol nm^2). The last configurations emerged from these simulations, that in all cases retained the folded hairpin structure, were used as the starting configurations for the production runs. For the 27-mer models the production trajectories were run for 200 ns at three different temperatures, $T = 300$, 340, and 380 K, of uninterrupted dynamics whereas the 11-mer models were simulated using the temperature replica-exchange method (see below).

2.3. Molecular dynamics protocol

The molecular dynamics package GROMACS version 4.5.5 [43] was used to simulate all systems, with a time step of 0.002 ps and periodic boundary conditions applied in all three dimensions. The electrostatic forces were evaluated by the Particle-Mesh Ewald method [44] (with real-space cut-off of 1.0 nm, grid spacing of 0.12 nm, and quadratic interpolation) and the Lennard–Jones forces by a cutoff of 1.0 nm (with long range dispersion corrections for the energy and pressure). The system was maintained at a constant temperature by the velocity rescaling thermostat [45] (with a coupling time of 0.1 ps), and a pressure of 1.0 bar by the Berendsen barostat [46] (with a compressibility of 5×10^{-5} 1/bar and a coupling time of 1.0 ps). The SETTLE algorithm [47] was used to constrain bond lengths and angles of the water molecules, whereas the oligonucleotides covalent bond distances were constrained using the LINCS algorithm [48]. The oligonucleotides and sodium cations ($\sigma_{Na+} = 0.333$ nm and $\in_{Na+} = 0.0116$ kJ/mol) were represented by the AMBER99 force field [49] and the solvent water molecules were described by the TIP3P model [50].

2.3.1. Temperature replica-exchange simulations

We carried out replica-exchange simulations for the RNA and hybrid 11-mer nucleotides. Eleven replicas at different temperatures, evenly distributed between 300 K and 340 K (thus, with a 4 K gap), were constructed. After periods of 5000 steps (i.e., 10 ps) of uninterrupted dynamics, Monte Carlo moves attempting to exchange the trajectories between neighboring replicas were performed. For both systems, the total simulation time for each replica was 30 ns. This resulted in 2337 and 2290 successful Monte Carlo temperature exchanges between the replicas (which is 8% exchange probability). In Fig. S1 in the supplementary material we exhibit the distributions of the potential energies of the different trajectories at each temperature indicating that there are significant overlaps between neighboring replicas.

3. Results and discussion

3.1. Untruncated 27-mer oligonucleotides

We simulated for 200 ns the untruncated NMR model of the RNA and hybrid oligonucleotides at three different temperatures: 300, 340, and 380 K. In all trajectories we did not observe any opening of the loop structure. This is likely a consequence of the presence of the 11 base-paired segment forming the stem (which are closed by two G:C base-pairs). In Fig. 2 we display the root mean squared deviations (RMSD) of the atoms of the oligonucleotides from the NMR structure that was taken for performing the simulations. The trajectories at 300 K are characterized by relatively small values of the RMSD, except for two spikes in the case of the hybrid which are a result of conformations in which the double-stranded helix is more elongated (reminiscent of that at higher temperatures). An average of 0.37 nm and 0.36 nm of the RMSD is observed for the RNA and hybrid oligomers, respectively. However, at $T = 340$ K, the curves indicate that there is a transition to a different state characterized by an RMSD value of around 1.0 nm. This transformation passes temporarily through a state with an RMSD of around 0.7 nm in the case of the RNA (see snapshot in Fig. S2), whereas it transforms directly in the case of the hybrid. Direct transformations are observed at $T = 380$ K and the transitions occur at shorter times. In fact, for the hybrid the transformation is within the first 1.5 ns whereas for the RNA it is after 40 ns. It is not clear whether these values are representative, nevertheless, it is interesting to point out that a larger kinetic stability of the loop motif for the RNA backbone was found by free energy calculations on a shorter sequence [27]. Note that the experimental NMR study deposited thirteen conformers in the Protein Data Bank. However, the difference between the structures of these conformers relative to the fluctuations observed in the simulations is quite small. This is shown in Fig. S3 where the RMSD calculations are performed also with respect to three other NMR conformers.

In Fig. S4 we plot the corresponding radius of gyration. These graphs indicate that the states with the larger RMSD values correspond also to states with larger radius of gyration. Snapshots of these states are given in Fig. 3. For both model systems, the two states do exhibit a general conformation of a hairpin. However, the state with the larger RMSD is elongated (hence, the larger value of the radius of gyration) with a smaller number of base-pairings, and these base-pairs are tilted. In addition, the shape of the double-helix is lost. In Table 1 we calculate the number of hydrogen bonds between different groups of the oligonucleotides. Considering the entire nucleotide chain, there are more hydrogen bonds within the RNA than within the hybrid. For example,

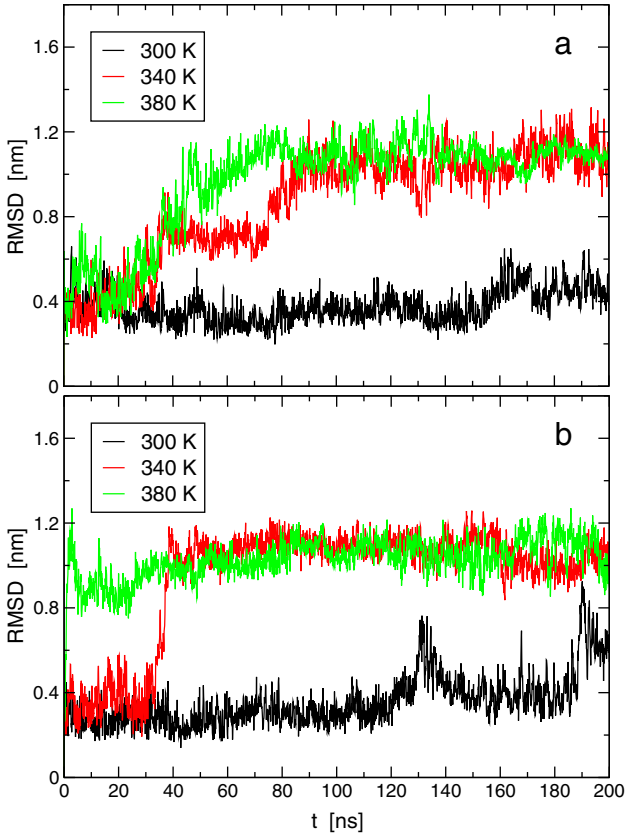

Fig. 2. The RMSD of all atoms of (a) the RNA and (b) the hybrid 27-mer oligonucleotides at three different temperatures. In the calculations of these curves, all the atoms of the oligonucleotide along the trajectories were fitted to the NMR structure (first conformer deposited in the PDB).

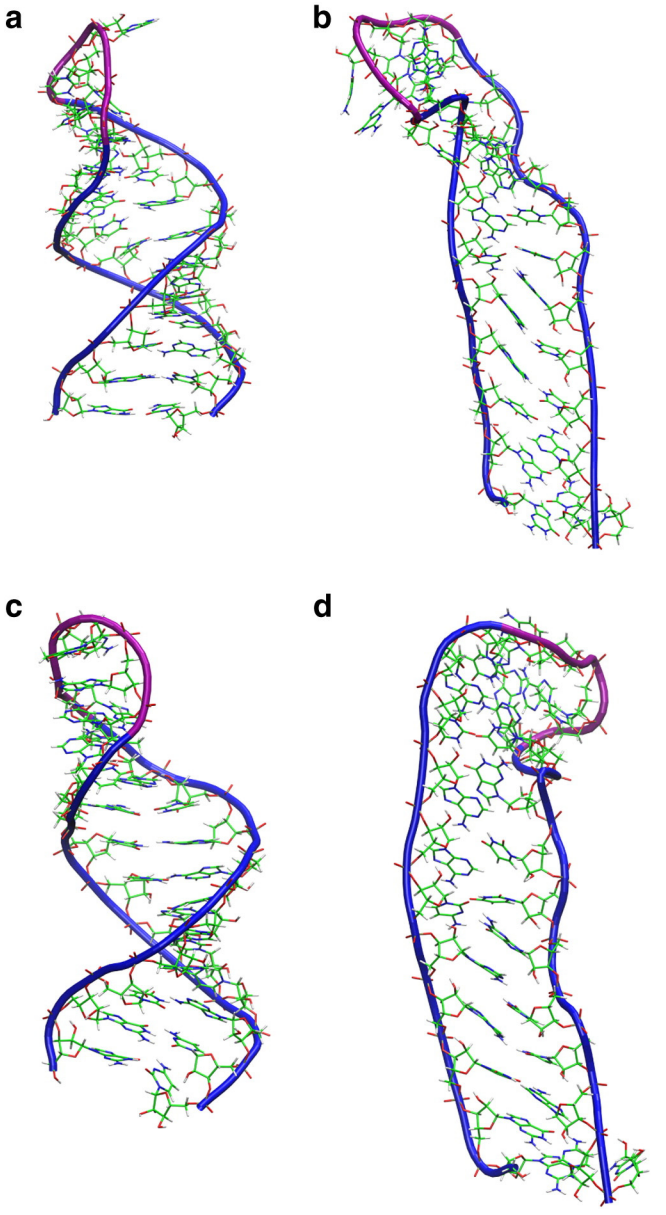

Fig. 3. Snapshots from the simulations at 340 K of (a) the folded ($t = 10.0$ ns, RMSD = 0.34 nm, and $R_g = 1.54$ nm) and (b) the stretched ($t = 171.6$ ns, RMSD = 1.12 nm, and $R_g = 1.98$ nm) conformations of the RNA hairpin. Analogous plots for the hybrid are shown in (c) and (d), for the folded ($t = 12.0$ ns, RMSD = 0.25 nm, and $R_g = 1.53$ nm) and stretched ($t = 124.4$ ns, RMSD = 1.12 nm, and $R_g = 1.88$ nm) conformations, respectively.

Table 1
The average number of hydrogen bonds between two groups of atoms, A and B, of the RNA and hybrid oligonucleotides at different temperatures. The seven nucleotides, 11–17, that underwent the mutation ribose → deoxyribose include the pentaloop and one nucleotide on each side. Also indicated are the corresponding values of the first conformer of the NMR structure deposited in the PDB, NMR-1, as well as, the average over the thirteen NMR structures, NMR-av. A hydrogen bond is defined by a donor–acceptor cutoff distance of 0.35 nm and a donor–hydrogen–acceptor angle larger than 150°.

A [nucleotides]	B [nucleotides]	NMR-1	NMR-av	RNA			Hybrid		
				300 K	340 K	380 K	300 K	340 K	380 K
1–27	1–27	31	31.4	35.9 ± 1.0	37.3 ± 4.5	33.4 ± 2.3	32.5 ± 4.1	36.1 ± 3.4	33.3 ± 1.1
11–17	11–17	7	7.3	7.8 ± 0.7	4.9 ± 1.2	5.9 ± 0.8	4.6 ± 3.1	3.6 ± 1.1	2.1 ± 1.3
11–17 only 2′-OH	11–17 excl. 2′-OH	1	1.9	3.6 ± 0.2	3.2 ± 0.3	3.3 ± 0.2	–	–	–
11–17 only 2′-OH	11–17 only sugars	0	0.54	2.4 ± 0.5	1.9 ± 0.7	1.9 ± 0.2	–	–	–
11–17 only 2′-OH	11–17 only bases	0	0.15	0.5 ± 0.6	0.5 ± 0.4	0.5 ± 0.2	–	–	–
11–17 only 2′-OH	11–17 only phosphates	1	1.2	0.7 ± 0.2	0.8 ± 0.1	0.9 ± 0.7	–	–	–
11–17 only 2′-OH	11–17 only 2′-OH	0	0	<0.05	<0.05	<0.05	–	–	–

at $T = 300$ K a difference of 3.4 hydrogen bonds is observed. This difference decreases rapidly at higher temperatures and for $T = 380$ K becomes negligible. In the hybrid, seven of the 2′-hydroxyls are missing around the loop-region (nucleotides 11 to 17) which is likely to be the reason for this larger number of hydrogen bonds in the RNA system. Indeed, as can be seen in the table, the 2′-hydroxyls in the loop region form hydrogen bonds with the sugar, phosphate, and base groups. The numbers with the sugars are larger than those with the phosphates or the bases. However, hydrogen bonds between the 2′-hydroxyls and sugar groups (mostly of adjacent nucleotides) form also in the stem. The unique behavior in the loop region is the formation of hydrogen bonds also with the phosphate groups (also of adjacent nucleotides) and with bases (mainly of non-adjacent nucleotides) which hardly exist in the stem. The hydrogen bonds of the 2′-OH with the bases were argued to contribute substantially to the stability of the hairpin conformation [27], however, it is possible that the hydrogen bonds with the adjacent phosphate groups also facilitate the loop conformation. Of the hydrogen bonds between the 2′-OH and the bases, an important contribution is obtained from the 2′-OH (acting as a donor) of the nucleotide at the first position of the pentaloop (G12) and N7 of adenine at the fourth position (A15). Other important contributions are the interactions formed between N6 (donor) of adenine at the fourth position and 2′-OH of the first position, as well as, between N2 (donor) of guanine at the first position and 2′-OH of uracil in the middle of the loop (U14). These types of intraloop hydrogen bonds induce bending of the chain and thereby augment the stability of the hairpin. The number of hydrogen bonds in the loop-region in which the 2′-OH is acting as, both, the acceptor and the donor is negligible.

As mentioned above, there is a correlation between the presence of the 2′-OH and the puckering of the ring of the sugar. To describe the type of the puckering of the sugar rings we adopted the definition of the pseudorotation phase angle, P, introduced by Altona and Sundaralingam [51,52],

$$P = \tan^{-1}\left[\frac{(\nu_4+\nu_1)-(\nu_3+\nu_0)]}{2\nu_2(\sin 36^\circ + \sin 72^\circ)}\right], \quad (1)$$

where the five cyclic ribose torsion angles are defined as follow: ν_0 = C4′–O4′–C1′–C2′; ν_1 = O4′–C1′–C2′–C3′; ν_2 = C1′–C2′–C3′–C4′; ν_3 = C2′–C3′–C4′–O4′; ν_4 = C3′–C4′–O4′–C1′. Note that describing the puckering by the distance between the phosphorus atom and the plane between two neighboring nucleotides [53] is not possible in the loop region because the bases are not stacked vertically as they do in a regular double-helix conformation. Based on experimentally resolved structures, it has been observed that typical C3′-endo state exhibits the north range of pseudorotation values, $-1^\circ \le P \le 34^\circ$, whereas the C2′-endo state exhibits the south range, $137 \le P \le 194^\circ$ [54]. In Table 2 we display the average values of P for the sugar groups of the five nucleotides of the pentaloop. For both, the RNA and hybrid oligomers, the pseudorotation angle corresponds to the C3′-endo conformation for all the temperatures studies. The values observed are in a relatively small range of 0.8° and 11.2°. As a reference, in the canonical A-form double-helix conformation $P = 13.1^\circ$, whereas in the B-form $P = 191.6^\circ$. In Fig. S5 and Fig. S6 we display the values of P along the trajectories. In general, fluctuations with small magnitudes are observed except for the uracil nucleotide at the middle of the loop in the RNA oligomer. The free energy barrier for the transition between C3′-endo and C2′-endo is estimated to be around 9 kJ/mol [54]. Therefore, we conjecture that the preference for the C3′-endo puckering is not a kinetically trap state of the starting conformation, but is a result of the imposed conformation of the backbone atoms in the loop region (however, the loop conformation itself can be a kinetically trapped state for the hybrid oligonucleotide). For comparison, in the stem region of the RNA hairpin, the nucleotides C6 and G22, forming a base-pair, have pseudorotation angle values of 5.8 and 2.9, respectively, which again represent the A-form helix conformation.

The conformation of the backbone atoms is described by several dihedral angles. Among them is the δ-dihedral, C5′–C4′–C3′–O3′, which exhibits different values in RNA (A-form) and DNA (B-form) double-helix. In the A-form, the values of δ range from 79° to 84° whereas in the B-form they range from 128° to 143° [53]. In Fig. 4 we plot the distributions of the values of δ for the five nucleotides of the pentaloop. For both nucleotides, the distributions are bimodal in which each peak represents either the A-form or the B-form conformation. The figure indicates that, in general, the values of δ for the nucleotides at the 5′ end of the loop are characterized more by the RNA values, whereas, those towards the 3′ end are characterized more by the DNA values. Within this trend, the difference between the RNA and the hybrid oligomers is that in the latter there is an increase in the amplitudes of the B-form helix. An exception to the bimodal distribution is the behavior of the δ of T14 and A15 of the hybrid that exhibits a unimodal distribution (the shape of the former is broad and non-Gaussian). As a reference, we plot in Fig. S7 in the Supplementary material the distribution of δ for two base-pairs in the stem of the RNA oligomer. The values observed in the stem exhibit almost exclusively the values for the A-form helix. The A-form character is also observed for the stem of the hybrid. Thus, one can conclude that

Table 2
The sugar puckering pseudorotation angle, P, of the nucleotides of the pentaloop for the 27-mer RNA and hybrid oligonucleotides. All values are given in degrees.

Nucleotide	RNA			Hybrid		
	300 K	340 K	380 K	300 K	340 K	380 K
G12	2.4 ± 0.3	3.2 ± 0.9	5.5 ± 0.4	4.1 ± 1.1	5.9 ± 0.7	6.1 ± 0.8
C13	6.0 ± 0.4	7.2 ± 0.7	4.5 ± 0.3	8.5 ± 1.3	0.8 ± 1.0	7.5 ± 0.3
U14/T14	11.2 ± 2.5	7.8 ± 1.6	8.9 ± 0.7	3.2 ± 8.1	1.3 ± 1.9	7.5 ± 0.5
A15	2.7 ± 1.3	3.1 ± 0.5	3.9 ± 0.9	9.5 ± 1.4	9.0 ± 1.8	6.8 ± 0.8
A16	4.0 ± 2.6	5.4 ± 0.6	2.5 ± 1.0	5.8 ± 0.5	7.7 ± 2.1	6.1 ± 1.5

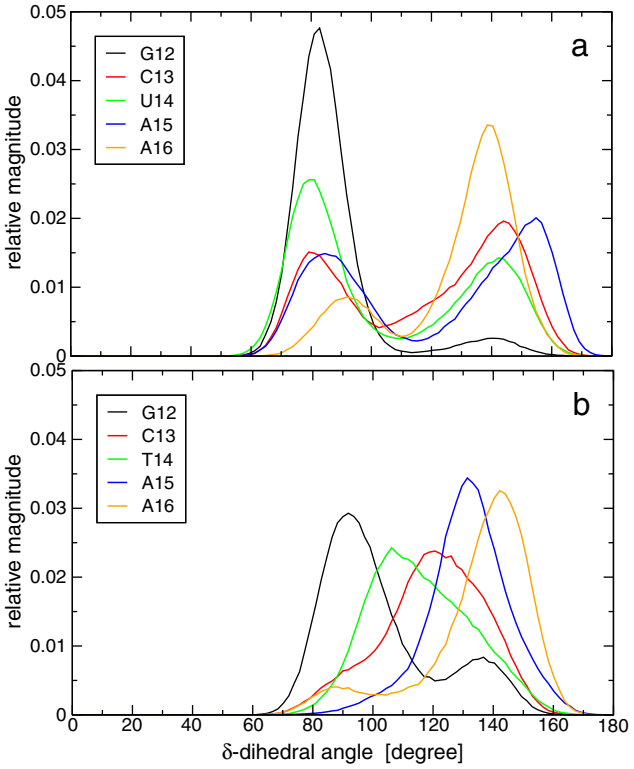

Fig. 4. The normalized distribution of the δ-dihedral angle of the five nucleotides of the pentaloop for (a) the RNA and (b) the hybrid 27mer nucleotides at $T = 300$ K.

the observation of the B-form (in addition to the A-form) values of the δ-dihedrals in the RNA chain is characteristic to loop regions. We also analyzed the distributions of the α, γ, ϵ, and χ backbone dihedrals (figures not shown), however, we could not clearly identify a difference between the behavior of the RNA compared with that of the hybrid.

3.2. Truncated 11-mer oligonucleotides

In order to observe a spontaneous opening of the hairpin loop during the simulations, and preferably several such events, we shortened the stem from 11 base-pairs to 3 base-pairs. This shortening significantly decreased the attractions within the stem and therefore the loop has a larger probability to open. To further facilitate the opening of the loop we performed replica-exchanged simulations within the temperature range of 300 K and 340 K. Our aim is to elucidate the influence of the hydroxyls of the ribose groups on the ability of the oligonucleotides to form a loop. To this end, we considered three descriptors to characterize the degree of the loop-opening; the RMSD with respect to the starting hairpin conformation (shown in Fig. S8), the radius of gyration (Fig. S9), and the distance between the C3′ atom of the third and ninth nucleotides (Fig. 5). In general, all descriptors display similar behavior indicating that the loop region of the hybrid opens to a greater extent than that of the RNA. Fig. S8 and Fig. S9 indicate that although the hybrid has a larger propensity to extend its loop, the closed-state of the hybrid is characterized by a smaller RMSD and radius of gyration values than those of the RNA. This behavior is also observed using constrained dynamics [27] and it is probably due to the fact that the hybrid oligonucleotide is more hydrophobic in the absence of the 2′-OH groups. Fig. 5 demonstrates that the average value of the distance d is the same for the closed-state in both oligomers, however whereas, the RNA loop exhibits both extensions and contractions (thus, larger and smaller d values, respectively), the hybrid mostly displays the extensions. Histograms of these three descriptors are shown in Figs. S10, S11, and S12 for $T = 300$, 320, and 340 K.

In search for cut-off values of the different descriptors to quantify the extent of the loop-opening we found that the most faithful criterion is the C3′(3)–C3′(9), d, distance. More specifically, the radius of gyration can sometimes exhibit relatively small values for opened (extended)-state loops in which the end (stem) nucleotides point toward each other. Alternatively, it can also exhibit relatively large values for closed-state loops in which the end nucleotides point away from each other. The RMSD criterion also suffered in some cases from inaccuracies between its values and the extent of the loop-opening. In Fig. 6 we

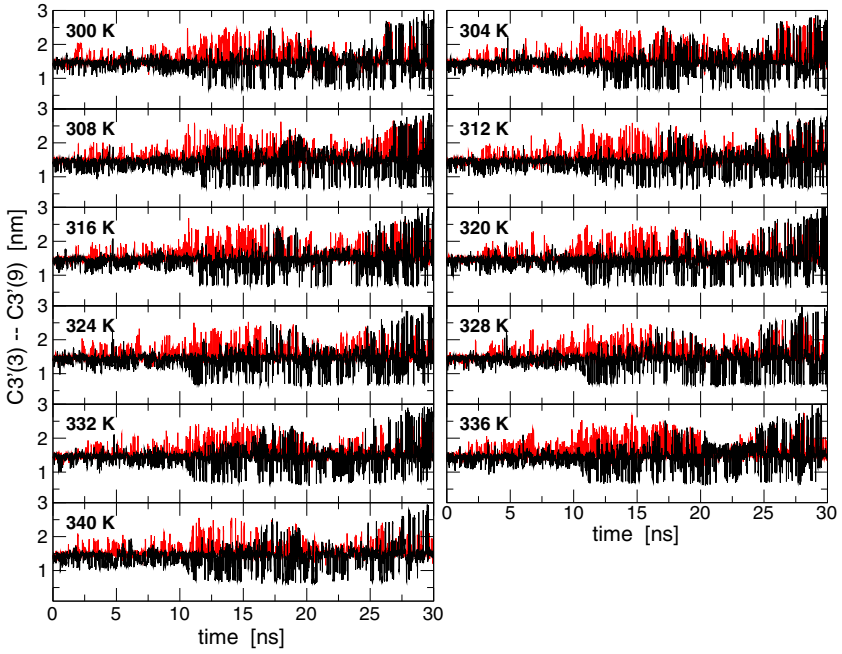

Fig. 5. The distance between the C3′ atom of the third and ninth residues for the truncated 11-mer nucleotides (black curve is for the RNA whereas the red is for the hybrid) as a function of time. The different temperatures shown are the 11-replicas employed in the replica-exchange simulations. (For interpretation of the references to color in this figure legend, the reader is referred to the web version of this article.)

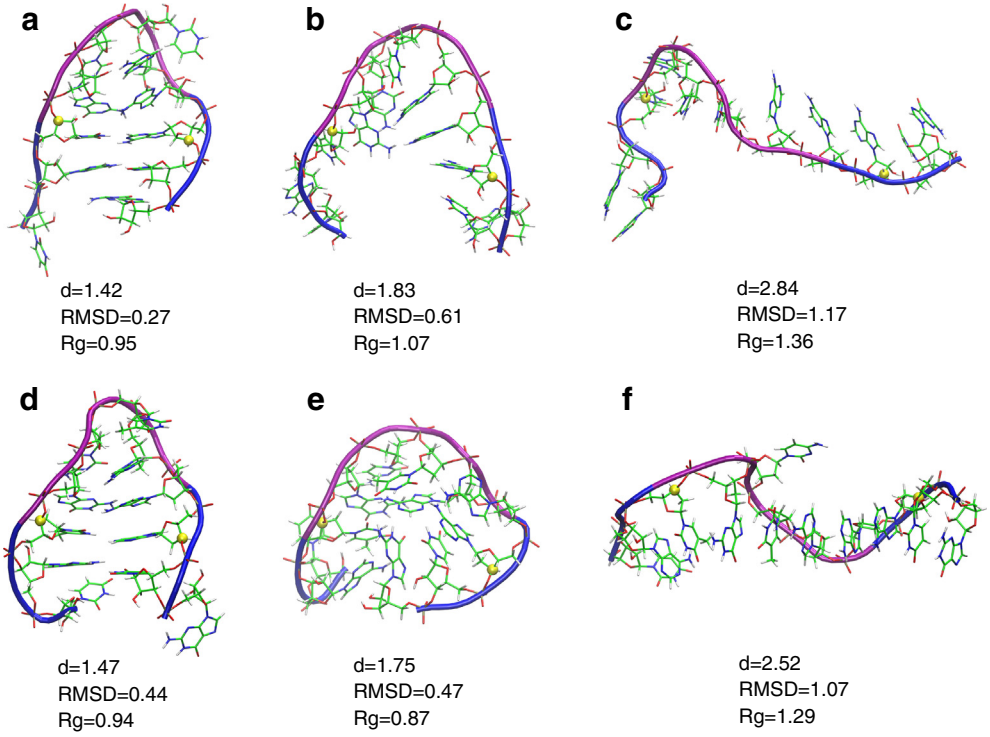

Fig. 6. Snapshots from the replica exchange simulations of the RNA (a–c, top panel) and hybrid (d–f, lower panel) oligonucleotides for different chain conformations at $T = 340$ K. The frames in (a) and (d) display hairpins in which four bases of the stem are paired, the frames in (b) and (e) display hairpins without base-pairing, and the frames in (c) and (f) display extended chains. Below each conformation the corresponding distance, d, between the C3′ atoms of the third and ninth residues (shown as yellow balls), RMSD, and radius of gyration, R_g, are indicated. The backbone of the pentaloop is depicted in magenta whereas that of the stem in blue. (For interpretation of the references to color in this figure legend, the reader is referred to the web version of this article.)

display three instantaneous conformations for each oligonucleotide along with the value of each descriptor. Note that in snapshots (d) and (e) the radius of gyration is smaller for the conformer with the more opened loop (the one in snapshot (e)) and the RMSD value is almost the same. The radius of gyration is also not an accurate descriptor for the degree of the extension of the loop in snapshots (a) and (b).

The C3′(3)–C3′(9) distance is the most direct measure for the magnitude of the loop-opening. From visual inspections of the conformations along the trajectories we noticed that the value of d has to be larger than 1.9 nm in order to represent an opened-state of the loop. This can also be seen in snapshots (b) and (e) in Fig. 6 that are characterized by the values of d just below 1.9 nm in which the loop region resembles more of the closed-state than the opened-state. We further analyzed the distributions of d of all replicas (three are shown in Fig. S10) and found that the closest minimum to discriminate between a closed and an opened states of the loop is at $d = 2.0$ nm.

Applying the above mentioned cut-off of d, we calculate in Fig. 7 the percentage of time in which the loop is in an extended-state for all replica (discarding the first 3 ns). At all temperatures, there are more extended states in the hybrid than in the RNA indicating that the RNA backbone, and in particular the 2′-OH, stabilizes the closed conformation of the loop. At $T = 300$ K, the percentages are 3.9 and 7.7 for the RNA and the hybrid, respectively. Assuming a two-state model, the value of the relative free energy change for opening the loop is $\Delta\Delta G = -RT \ln[K_{RNA}/K_{HYB}] = 1.8$ kJ/mol (where K is the equilibrium constant between the opened and closed states). This value is within the range of the 4.2 ± 6.5 kJ/mol obtained by potential of mean force calculations but much lower than the 23.8 ± 4.1 kJ/mol obtained by alchemical mutations [27]. Thus, the results from the replica-exchange simulations support the smaller value for the excess stability of the RNA loop structure relative to the hybrid. It should be noted that in the previous free energy calculations, constraints or restraints were applied to the chain to ensure the opened or closed states, however, there was no need to make an assumption in regard to the number of states of the system as is the case here.

In contrast to the behavior of the 27-mer, the oligonucleotides of the truncated models do exhibit spontaneous loop openings. These extensions of the chain can be coupled to changes in the sugars puckering. To this end, we also analyzed the pseudorotation angle, P, of the pentaloop nucleotides for these oligonucleotides and the results are presented in Table S1. However, the behavior exhibited by the truncated models is exactly the same as for the full length oligomers. This means, the sugars of all five nucleotides, of the RNA and hybrid, display

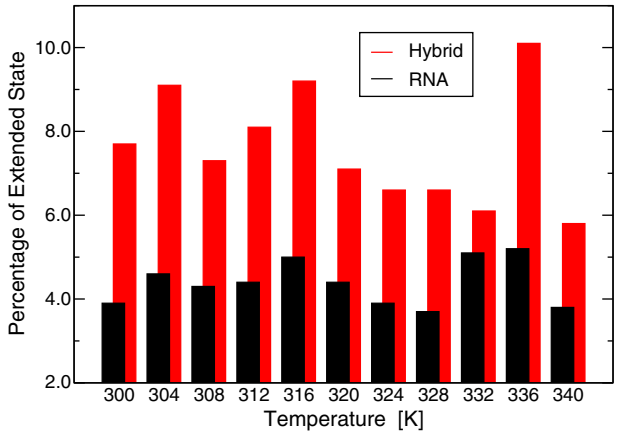

Fig. 7. The percentage of the extended state of the oligonucleotides at the different temperatures of the replica simulations.

the C3′-endo state characteristic to the A-form conformation. The similarity between the truncated and untruncated oligonucleotides is also observed for the behavior of the δ backbone dihedral angle (shown in Fig. S13). Similar to the 27-mer RNA, the 11-mer RNA also displays bimodal distributions around values that are characteristic for the A-form and B-form conformations. However, the hybrid of the 11-mer exhibits a clearer tendency towards the B-form, and in fact, for all nucleotides of the pentaloop, except for the first position (G4), the distributions are unimodal with values of the maxima larger than 130°. Further analyses of the other backbone torsions indicate that for the other dihedrals in the pentaloop there is no clear distinction between the RNA and hybrid behavior. We demonstrate this for the χ dihedral, which is the torsion angle around the N-glycosidic bond (defined by O4′–C1′–N9/N1–C4/C2, for purines and pyrimidines, respectively) in Fig. S14. The backbone χ dihedral assumes values around −140° for the C3′-endo (A-form) conformation and in the range of $-110° < \chi < -60°$ for the C2′-endo (B-form) conformation [55]. From the distributions in Fig. S14, it is evident that some nucleotides exhibit the values corresponding to the A-form and other to the B-form, and that it is predominantly dependent on the position in the pentaloop rather than the presence or the absence of the 2′-hydroxyls. Note however, that the curves for G4 (first position of the loop) and A8 (last position) are much broader for the RNA than for the hybrid. This might be a consequence of the hydrogen bonds involving the 2′-OH that are formed within the pentaloop of the RNA but not of the hybrid.

As mentioned earlier, there are only two differences between the RNA and the hybrid; namely the absence of seven 2′-OH of the sugars and the presence of two thymines instead of uracils in the loop-region of the hybrid. Although, this study was not designed to address the effect of the methyl group of thymine (which differentiates it from uracil) we conjecture that it does not have a major role in the structural and dynamical differences observed in this study. It is more likely that the existence/absence of the 2′-OH is the reason for the larger kinetic and thermodynamic stability of the loop structure in the RNA hairpin. Why do the 2′-hydroxyls promote loop structures? One possible answer is the tendency of ribose backbones to adopt a different conformation than that of deoxyribose backbones and that conformation better facilitates the curvature of a loop. Indeed, there are several known differences between the conformations of RNA and DNA backbones, such as the puckering of the sugar rings and the values of several backbone dihedrals. However, these differences in conformations are established mostly in the structures of the double-helix (A-form versus B-form helices) and not in loop-regions. From the analyses of the sugar puckers and the backbone dihedral angles performed in this study the most significant difference in the loop region between the RNA and hybrid was that of the δ-dihedral. It is not clear, however, to what extent the behavior of this dihedral stabilizes the structure of the hairpin. Nevertheless, if this dihedral does contribute to the stability of the hairpin it is likely to be due to a conformation that facilitates the 2′-OH to form intraloop hydrogen bonds.

4. Conclusions

There are few examples showing that the hydroxyl groups of the ribose sugars in RNA form intra- or inter-chain hydrogen bonds and, thereby, stabilize secondary and tertiary structural elements that are unique for RNA. Among these structural motifs is the loop structure. The results presented in this paper support the role of 2′-hydroxyls in stabilizing loop structures. This was demonstrated on the particular case of the GCUAA pentaloop. However, absence of such stabilization for other sequences and/or loop lengths cannot be ruled-out. Although the magnitude of the stabilization that we observed is rather small, the difference in the population of the extended state conformation of the RNA and hybrid oligonucleotides is significant. The most dominant interaction inducing the excess stability of the RNA hairpin is a hydrogen bond between the 2′-OH at the first position of the loop and N7 of adenine at the forth position. Such hydrogen bond pattern introduces bending in the oligonucleotide chain that supports the conformation of a loop. Attempts to correlate the excess stability to the conformation of the sugar puckers or backbone dihedrals were not successful, except for the case of the δ-dihedral. In the RNA pentaloop, this dihedral displayed values that correspond to, both, RNA and DNA backbones, whereas in the hybrid pentaloop the values were mainly corresponding to those of a DNA backbone. It is tempting to conjecture that this difference in the behavior of the δ-dihedral facilitates the hydrogen bondings of the 2′-OH that stabilize the curvature of the loop.

Acknowledgments

This work has been funded with support from the Spanish Ministry of Science and Innovation, MICINN (grant number CTQ2010-20297) and the Basque Government, the ETORTEK program (BioGUNE2010, Expt. # IE10-275). Technical and human support provided by SGIker (USED SERVICES) (UPV/EHU, MICINN, GV/EJ, ESF) is gratefully acknowledged. The authors also thankfully acknowledge the computer resources and technical assistance provided by the Barcelona Supercomputing Center — Centro Nacional de Supercomputación.

Appendix A. Supplementary data

Supplementary data to this article can be found online at http://dx.doi.org/10.1016/j.bpc.2013.07.003.

References

[1] P. Svoboda, A.D. Cara, Hairpin RNA: a secondary structure of primary importance, Cell. Mol. Life Sci. 63 (2006) 901–908.
[2] P.C. Bevilacqua, J.M. Blose, Structures, kinetics, thermodynamics, and biological functions of RNA hairpins, Annu. Rev. Phys. Chem. 59 (2008) 79–103.
[3] C. Ban, B. Ramakrishnan, M. Sundaralingam, A single 2′-hydroxyl group converts B-DNA to A-DNA: crystal structure of the DNA-RNA chimeric decamer duplex d(CCGGC)r(G)d(CCGG) with a novel intermolecular G:C base-paired quadruplet, J. Mol. Biol. 236 (1994) 275–285.
[4] J. Liu, D.M. Lilley, The role of specific 2′-hydroxyl groups in the stabilization of the folded conformation of kink-turn RNA, RNA 13 (2007) 200–210.
[5] H.W. Pley, K.M. Flaherty, D.B. McKay, Model for an RNA tertiary interaction from the structure of an intermolecular complex between a GAAA tetraloop and an RNA helix, Nature 372 (1994) 111–113.
[6] J.H. Cate, A.R. Gooding, E. Podell, K. Zhou, B.L. Golden, C.E. Kundrot, T.R. Cech, J.A. Doudna, Crystal structure of a group I ribozyme domain: principles of RNA packing, Science 273 (1996) 1678–1685.
[7] P. Nissen, J.A. Ippolito, N. Ban, P.B. Moore, T.A. Steitz, RNA tertiary interactions in the large ribosomal subunit: the A-minor motif, Proc. Natl. Acad. Sci. U. S. A. 98 (2001) 4899–4903.
[8] M. Tamura, S.R. Holbrook, Sequence and structural conservation in RNA ribose zippers, J. Mol. Biol. 320 (2002) 455–474.
[9] G.W. Collie, S.M. Haider, S. Neidle, G.N. Parkinson, A crystallographic and modelling study of a human telomeric RNA (TERRA) quadruplex, Nucleic Acids Res. 38 (2010) 5569–5580.
[10] S.E. Butcher, A.M. Pyle, The molecular interactions that stabilize RNA tertiary structure: RNA motifs, patterns, and networks, Acc. Chem. Res. 44 (2011) 1302–1311.
[11] A.M. Pyle, T.R. Cech, Ribozyme recognition of RNA by tertiary interactions with specific ribose 2′-OH groups, Nature 350 (1991) 628–631.
[12] P.C. Bevilacqua, D.H. Turner, Comparison of binding of mixed ribose-deoxyribose analogues of CUCU to a ribozyme and to GGAGAA by equilibrium dialysis: evidence for ribozyme specific interactions with 2′ OH groups, Biochemistry 30 (1991) 10632–10640.
[13] M. Chastain, I. Tinoco, A base-triple structural domain in RNA, Biochemistry 31 (1992) 12733–12741.
[14] A.M. Pyle, F.L. Murphy, T.R. Cech, RNA substrate binding site in the catalytic core of the Tetrahymena ribozyme, Nature 358 (1992) 123–128.
[15] S.A. Strobel, T.R. Cech, Translocation of an RNA duplex on a ribozyme, Nat. Struct. Biol. 1 (1994) 13–17.
[16] H.W. Pley, K.M. Flaherty, D.B. McKay, Three-dimensional structure of a hammerhead ribozyme, Nature 372 (1994) 68–74.
[17] U. von Ahsen, R. Green, R. Schroeder, H.F. Noller, Identification of 2′-hydroxyl groups required for interaction of a tRNA anticodon stem-loop region with the ribosome, RNA 3 (1997) 49–56.
[18] D.E. Draper, Themes in RNA-protein recognition, J. Mol. Biol. 293 (1999) 255–270.
[19] U.F. Müller, D.P. Bartel, Substrate 2′-hydroxyl groups required for ribozyme-catalyzed polymerization, Chem. Biol. 10 (2003) 799–806.

[20] S.G. Landt, A.R. Tipton, A.D. Frankel, Localized influence of 2′-hydroxyl groups and helix geometry on protein recognition in the RNA major groove, Biochemistry 44 (2005) 6547–6558.
[21] F.H.-T. Allain, G. Varani, Structure of the P1 helix from group I self-splicing introns, J. Mol. Biol. 250 (1995) 333–353.
[22] E. Ennifar, A. Nikulin, S. Tishchenko, A. Serganov, N. Nevskaya, M. Garber, B. Ehresmann, C. Ehresmann, S. Nikonov, P. Dumas, The crystal structure of UUCG tetraloop, J. Mol. Biol. 304 (2000) 35–42.
[23] J.K. James, I. Tinoco, The solution structure of a d[C(TTCG)G] DNA hairpin and comparison to the unusually stable RNA analogue, Nucleic Acids Res. 21 (1993) 3287–3293.
[24] T. Sakata, H. Hiroaki, Y. Oda, T. Tanaka, M. Ikehara, S. Uesugi, Studies on the structure and stabilizing factor of the CUUCGG hairpin RNA using chemically synthesized oligonucleotides, Nucleic Acids Res. 18 (1990) 3831–3839.
[25] D.J. Williams, K.B. Hall, Experimental and theoretical studies of the effects of deoxyribose substitutions on the stability of the UUCG tetraloop, J. Mol. Biol. 297 (2000) 251–265.
[26] D.J. Williams, J.L. Boots, K.B. Hall, Thermodynamics of 2′-ribose substitutions in UUCG tetraloops, RNA 7 (2001) 44–53.
[27] A. Paladino, R. Zangi, Ribose 2′-hydroxyl groups stabilize RNA hairpin structures containing GCUAA pentaloop, J. Chem. Theory Comput. 9 (2013) 1214–1221.
[28] J. SantaLucia, R. Kierzek, D.H. Turner, Context dependence of hydrogen bond free energy revealed by substitutions in an RNA hairpin, Science 256 (1992) 217–219.
[29] A. Pérez, F.J. Luque, M. Orozco, Dynamics of B-DNA on the microsecond time scale, J. Am. Chem. Soc. 129 (2007) 14739–14745.
[30] F. Colizzi, G. Bussi, RNA unwinding from reweighted pulling simulations, J. Am. Chem. Soc. 134 (2012) 5173–5179.
[31] P.D. Dans, A. Pérez, I. Faustino, R. Lavery, M. Orozco, Exploring polymorphisms in B-DNA helical conformations, Nucleic Acids Res. 40 (2012) 10668–10678.
[32] M. Krepl, M. Otyepka, P. Banáš, J. Šponer, Effect of guanine to inosine substitution on stability of canonical DNA and RNA duplexes: molecular dynamics thermodynamics integration study, J. Phys. Chem. B 117 (2013) 1872–1879.
[33] J.L. Miller, P.A. Kollman, Theoretical studies of an exceptionally stable RNA tetraloop: observation of convergence from an incorrect NMR structure to the correct one using unrestrained molecular dynamics, J. Mol. Biol. 270 (1997) 436–450.
[34] E.J. Sorin, M.A. Engelhardt, D. Herschlag, V.S. Pande, RNA simulations: probing hairpin unfolding and the dynamics of a GNRA tetraloop, J. Mol. Biol. 317 (2002) 493–506.
[35] N.-J. Deng, P. Cieplak, Molecular dynamics and free energy study of the conformational equilibria in the UUUU RNA hairpin, J. Chem. Theory Comput. 3 (2007) 1435–1450.
[36] A.E. Garcia, D. Paschek, Simulation of the pressure and temperature folding/unfolding equilibrium of a small RNA hairpin, J. Am. Chem. Soc. 130 (2008) 815–817.
[37] A. Villa, E. Widjajakusuma, G. Stock, Molecular dynamics simulation of the structure, dynamics, and thermostability of the RNA hairpins uCACGg and cUUCGg, J. Phys. Chem. B 112 (2008) 134–142.
[38] G.R. Bowman, X. Huang, Y. Yao, J. Sun, G. Carlsson, L.J. Guibas, V.S. Pande, Structural insight into RNA hairpin folding intermediates, J. Am. Chem. Soc. 130 (2008) 9676–9678.
[39] P. Banáš, D. Hollas, M. Zgarbová, P. Jurečka, M. Orozco, T.E. Cheatham, J. Šponer, M. Otyepka, Performance of molecular mechanics force fields for RNA simulations: stability of UUCG and GNRA hairpins, J. Chem. Theory Comput. 6 (2010) 3836–3849.
[40] K. Sarkar, D.A. Nguyen, M. Gruebele, Loop and stem dynamics during RNA hairpin folding and unfolding, RNA 16 (2010) 2427–2434.
[41] N.-J. Deng, P. Cieplak, Free energy profile of RNA hairpins: a molecular dynamics simulation study, Biophys. J. 98 (2010) 627–636.
[42] R. Stefl, F.H.-T. Allain, A novel RNA pentaloop fold involved in targeting ADAR2, RNA 11 (2005) 592–597.
[43] B. Hess, C. Kutzner, D. van der Spoel, E. Lindahl, GROMACS 4: algorithms for highly efficient, load-balanced, and scalable molecular simulation, J. Chem. Theory Comput. 4 (2008) 435–447.
[44] T. Darden, D. York, L. Pedersen, Particle mesh Ewald: an N-log(N) method for Ewald sums in large systems, J. Chem. Phys. 98 (1993) 10089–10092.
[45] G. Bussi, D. Donadio, M. Parrinello, Canonical sampling through velocity rescaling, J. Chem. Phys. 126 (2007) 014101.
[46] H.J.C. Berendsen, J.P.M. Postma, W.F. van Gunsteren, A. DiNola, J.R. Haak, Molecular dynamics with coupling to an external bath, J. Chem. Phys. 81 (1984) 3684–3690.
[47] S. Miyamoto, P.A. Kollman, SETTLE: an analytical version of the SHAKE and RATTLE algorithms for rigid water models, J. Comp. Chem. 13 (1992) 952–962.
[48] B. Hess, H. Bekker, H.J.C. Berendsen, J.G.E.M. Fraaije, LINCS: a linear constraint solver for molecular simulations, J. Comp. Chem. 18 (1997) 1463–1472.
[49] J. Wang, P. Cieplak, P.A. Kollman, How well does a restrained electrostatic potential (RESP) model perform in calculating conformational energies of organic and biological molecules? J. Comp. Chem. 21 (2000) 1049–1074.
[50] W.L. Jorgensen, J. Chandrasekhar, J.D. Madura, R.W. Impey, M.L. Klein, Comparison of simple potential functions for simulating liquid water, J. Chem. Phys. 79 (1983) 926–935.
[51] C. Altona, M. Sundaralingam, Conformational analysis of the sugar ring in nucleosides and nucleotides. New description using the concept of pseudorotation, J. Am. Chem. Soc. 94 (1972) 8205–8212.
[52] B. Schneider, H.M. Berman, Computational studies of RNA and DNA, Challenges and Advances in Computational Chemistry and Physics, vol. 2, Springer, Dordrecht, The Netherlands, 2006. , (Ch. 1).
[53] X.-J. Lua, Z. Shakkedb, W.K. Olson, A-form conformational motifs in ligand-bound DNA structures, J. Mol. Biol. 300 (2000) 819–840.
[54] K. Arora, T. Schlick, Deoxyadenosine sugar puckering pathway simulated by the stochastic difference equation algorithm, Chem. Phys. Lett. 378 (2003) 1–8.
[55] W. Saenger, Principles of Nucleic Acid Structure, Springer-Verlag, New York, 1984.

Supporting Information:

Propensities for Loop Structures of RNA & DNA Backbones

Antonella Paladino[1] and Ronen Zangi[1,2,‡]

1. Department of Organic Chemistry I, University of the Basque Country UPV/EHU, Avenida de Tolosa 72, 20018, San Sebastian, Spain

2. IKERBASQUE, Basque Foundation for Science, 48011, Bilbao, Spain

July 10, 2013

‡ Email: r.zangi@ikerbasque.org

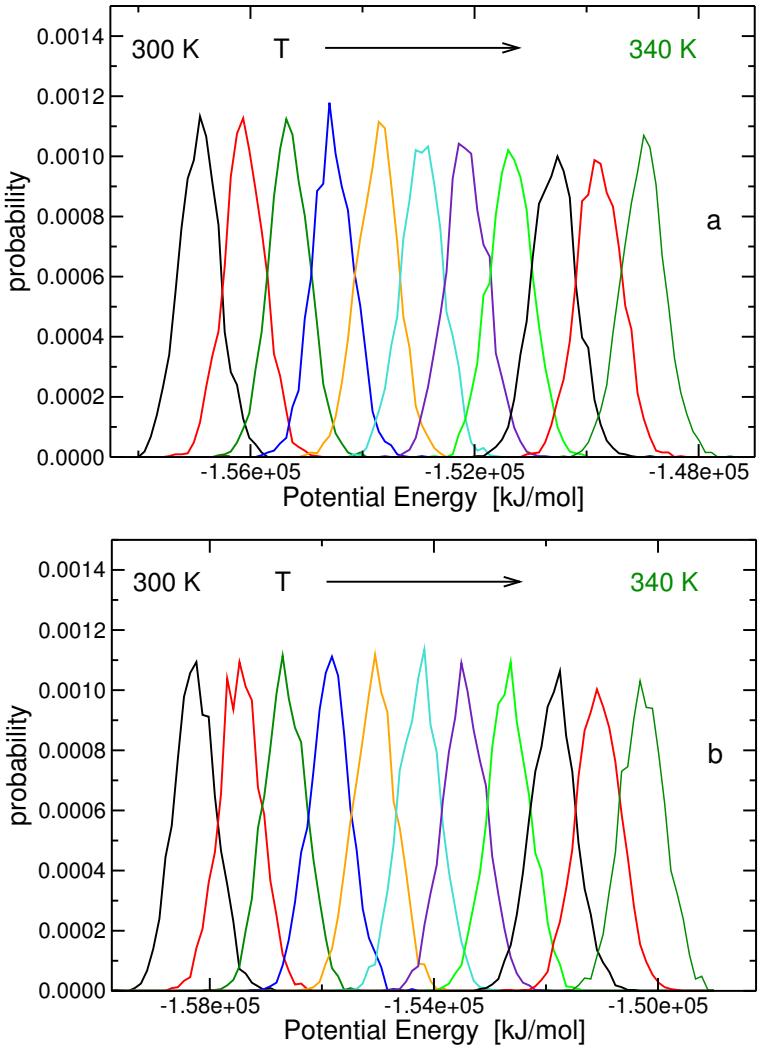

Figure S1: The distributions of the potential energies of the different replicas for the RNA (a) and hybrid (b) 11-mer oligonucleotides. In these replica-exchange simulations, there are 11 replicas evenly distributed from T=300 K (most left curve) to T=340 K (most right curve).

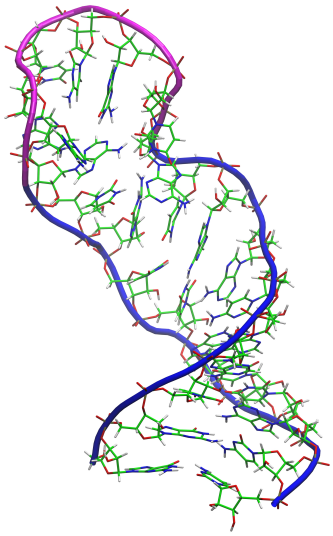

Figure S2: A snapshot of the intermediate state of the RNA oligomer observed at T=340 K in Fig. 2a. The snapshot is extracted from t=43.6 ns and is characterized by an RMSD value of 0.66 nm and radius of gyration of 1.61 nm.

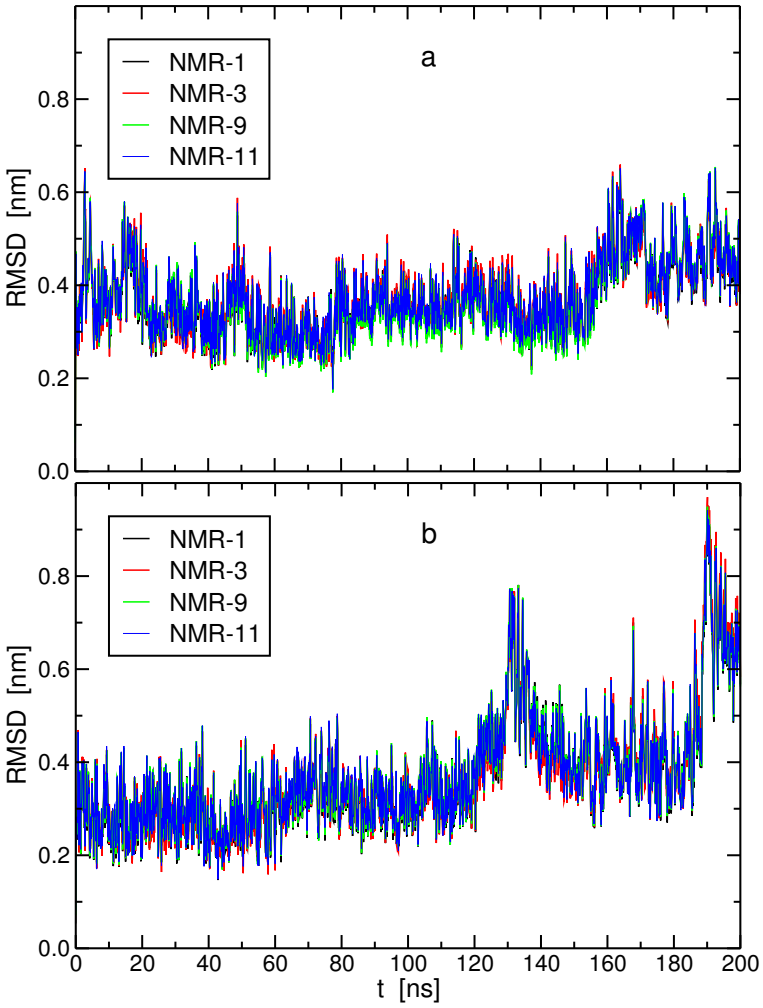

Figure S3: The RMSD of all atoms of (a) the RNA and (b) the hybrid 27-mer oligonucleotides at 300 K with respect to four NMR conformers deposited in the PDB.

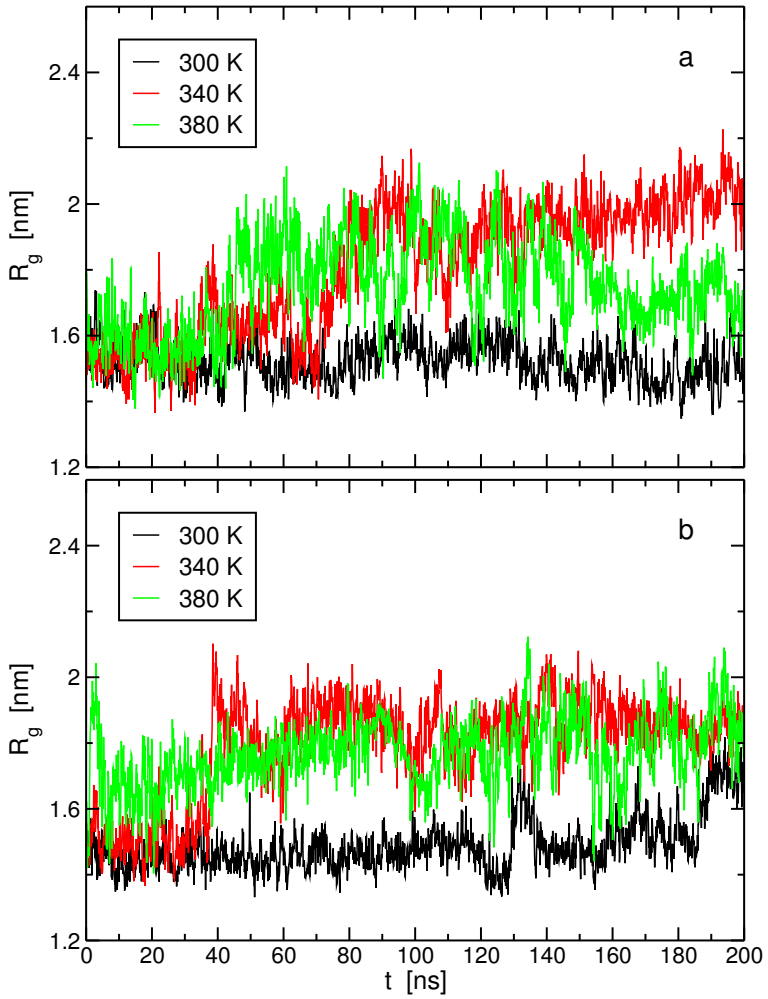

Figure S4: The radius of gyration of (a) the RNA and (b) the hybrid 27-mer oligonucleotides at three different temperatures.

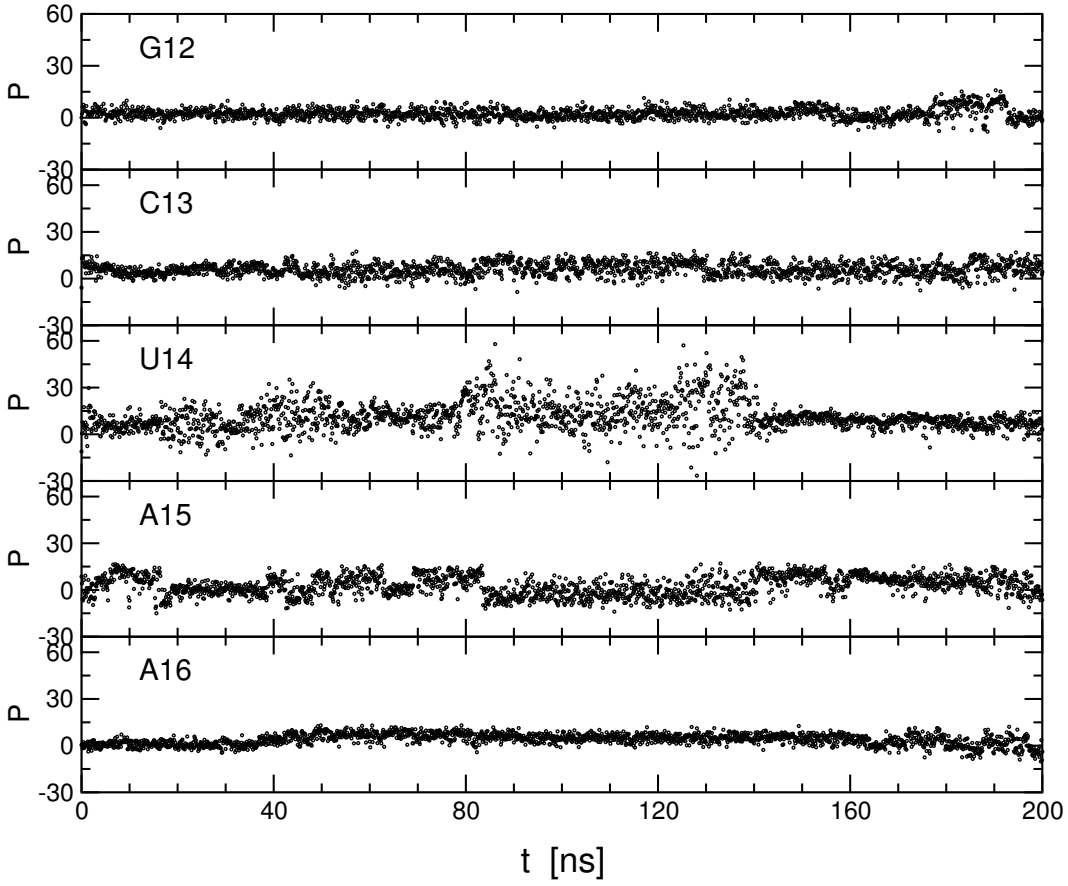

Figure S5: The sugar puckering pseudo rotation angle, P, for the 27-mer RNA oligonucleotide as a function of time. The values of P were calculated for the five nucleotides of the pentaloop for the simulation at T=300 K.

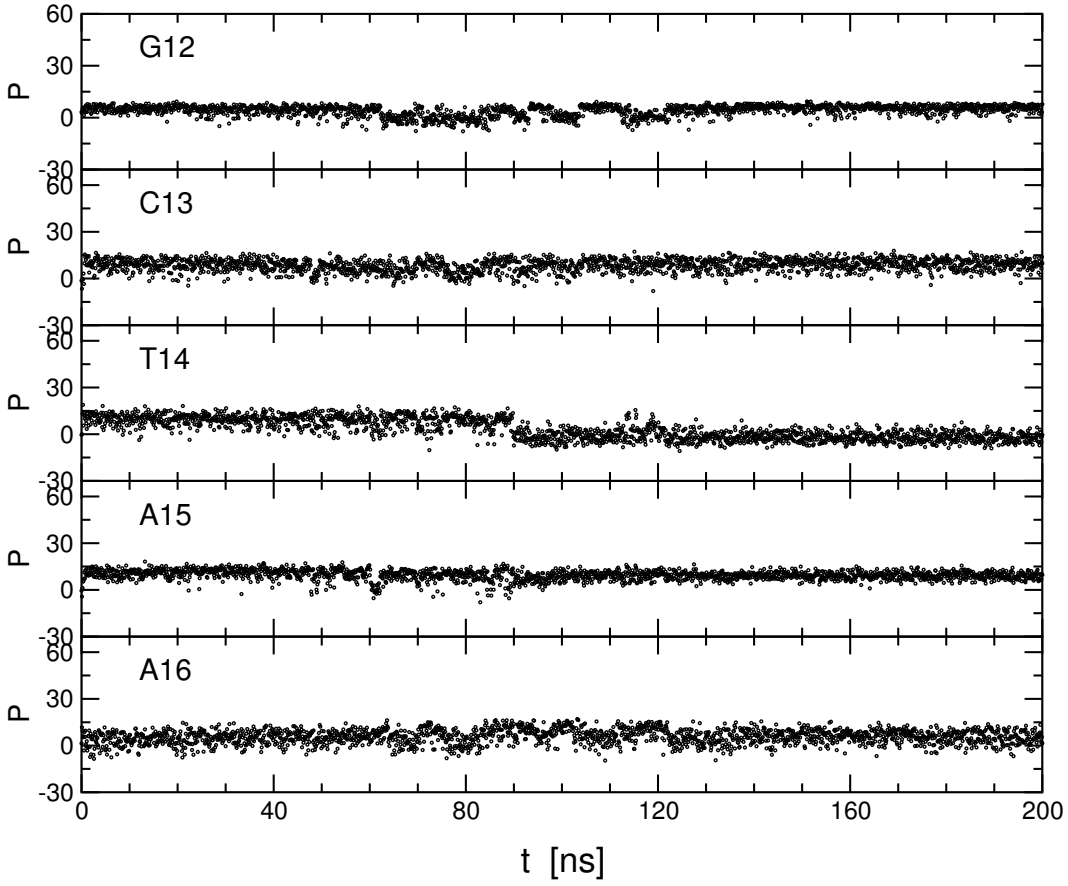

Figure S6: Same as Fig. S5 but for the hybrid 27-mer oligonucleotide.

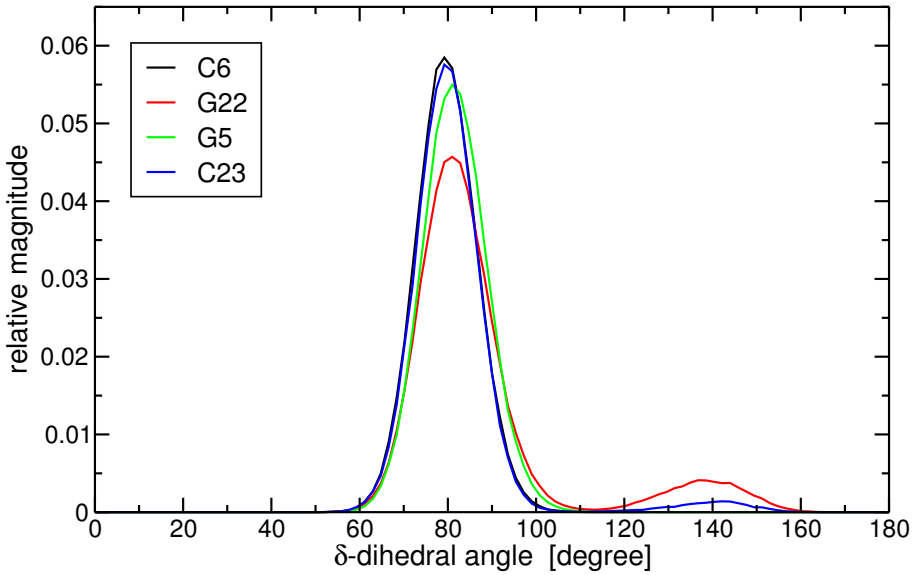

Figure S7: The normalized distribution of the δ-dihedral angle of four nucleotides that form two base-pairs in the stem of the RNA 27mer hairpin at T=300 K.

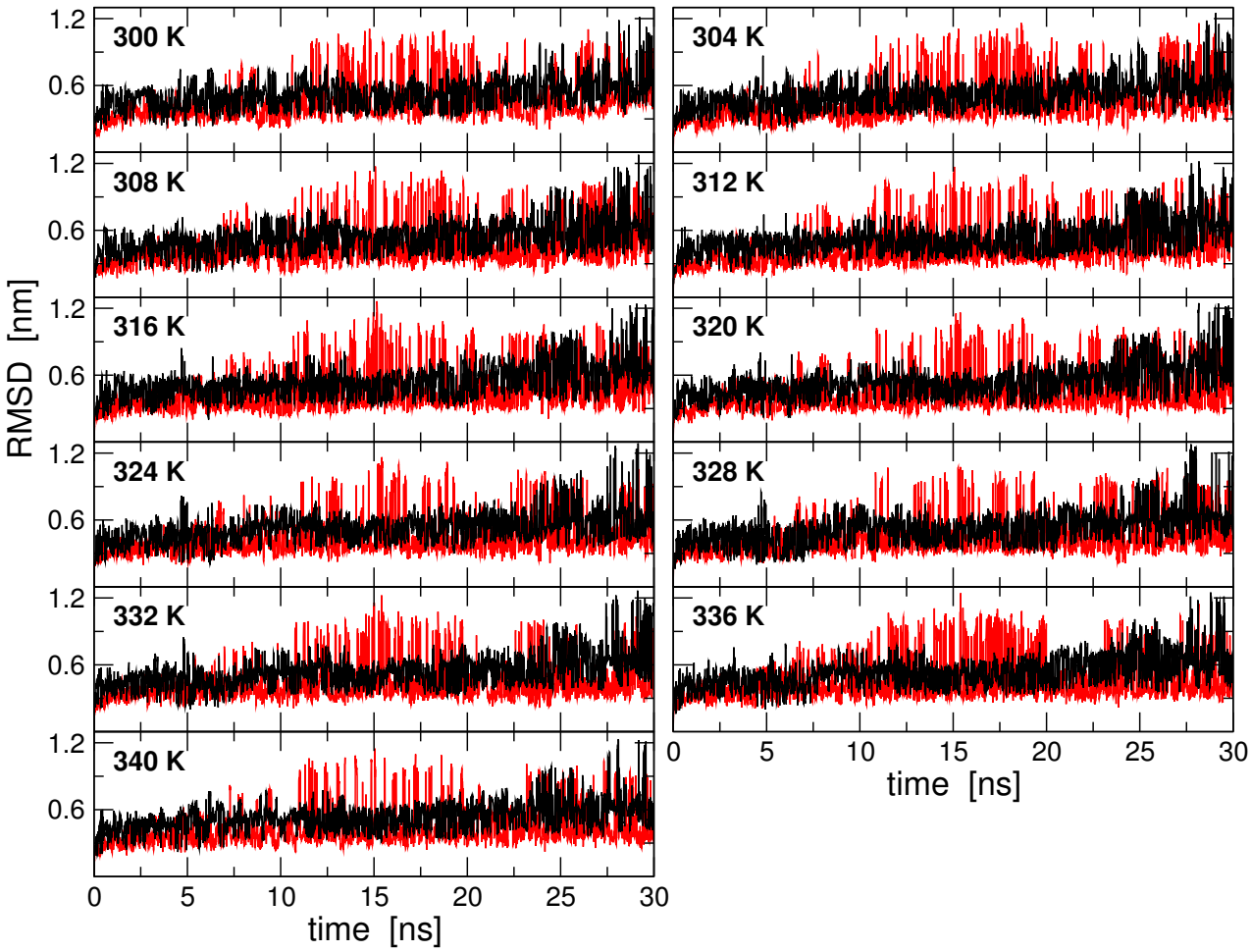

Figure S8: The RMSD of all atoms of the oligonucleotides (black curve is for the RNA and the red is for the hybrid) fitted and calculated relative to the starting (hairpin) conformations as a function of time. The different temperatures shown are the 11-replicas employed in the replica-exchange simulations.

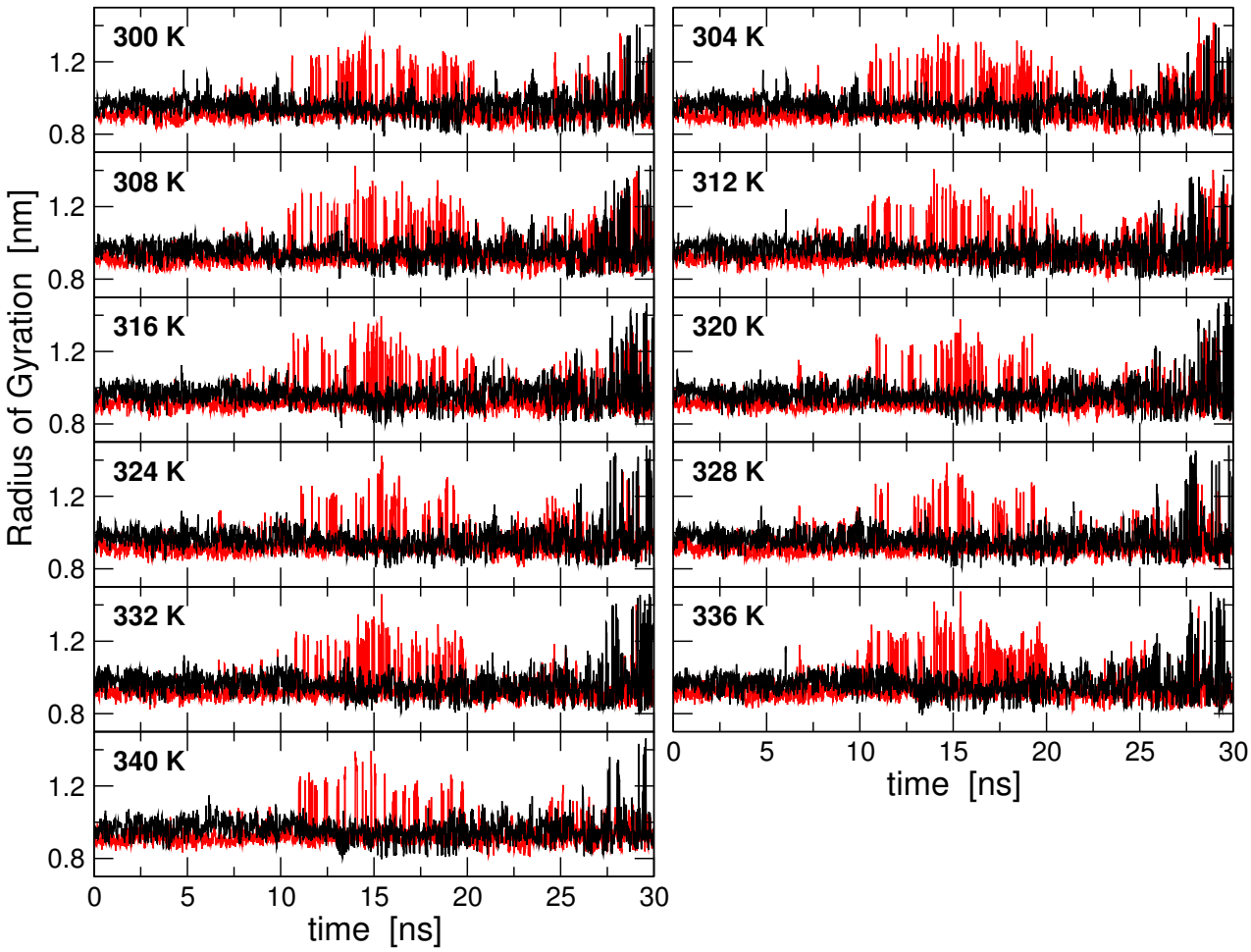

Figure S9: Same as Fig. S8 but for the radius of gyration of the oligonucleotide chains.

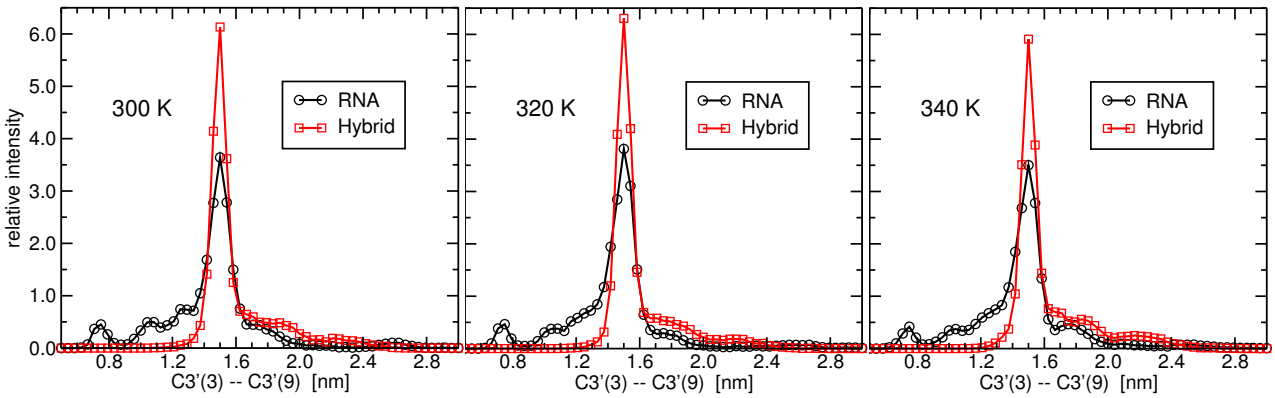

Figure S10: The normalized histograms of the distance between C3' of the third residue and C3' of the ninth residue (Fig. 5) for the 11-mer RNA and hybrid oligonucleotides at three different temperatures.

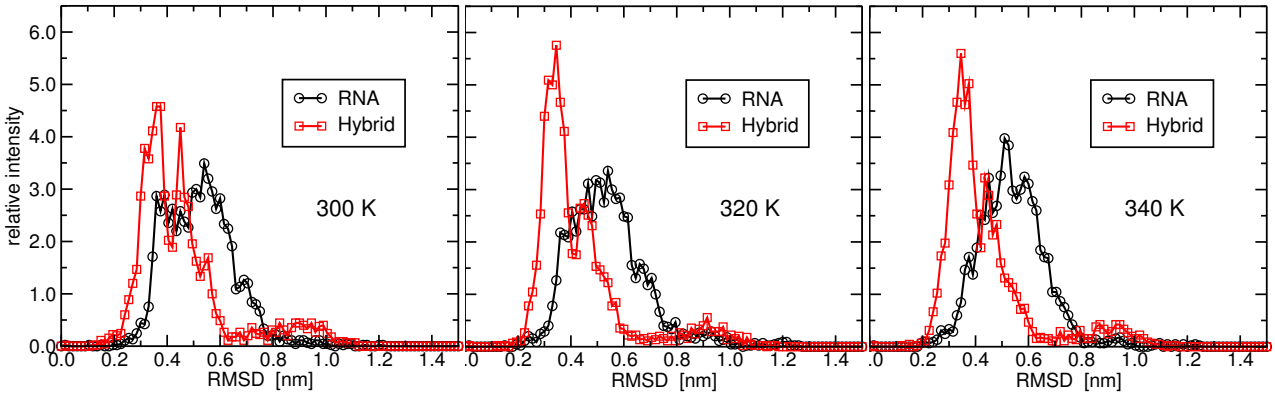

Figure S11: The normalized histograms of the RMSD (shown in Fig. S8) for the 11-mer RNA and hybrid oligonucleotides at three different temperatures.

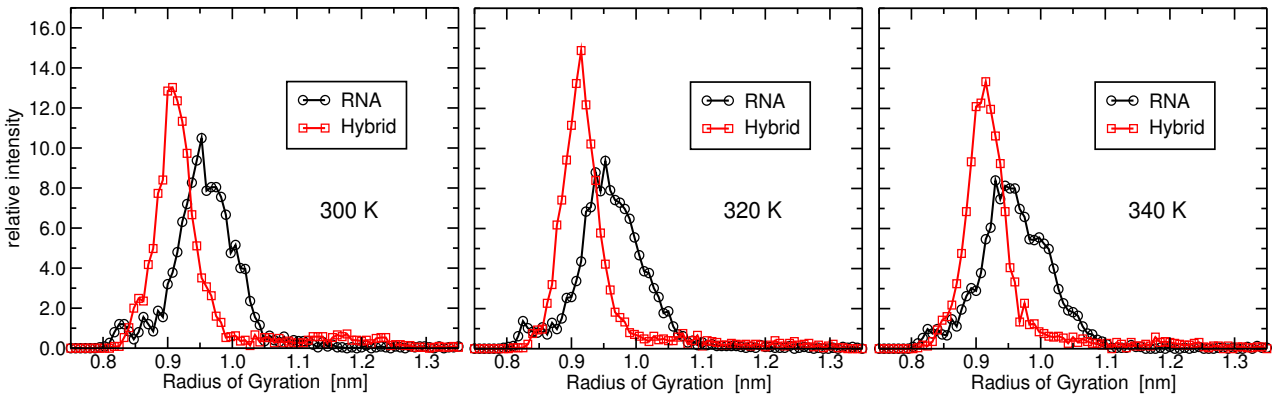

Figure S12: The normalized histograms of the radius of gyration (shown in Fig. S9) for the 11-mer RNA and hybrid oligonucleotides at three different temperatures.

Table S1: The average value of the sugar puckering pseudorotation angle, P, of the pentaloop for the RNA and hybrid 11-mer oligonucleotides at 300 K. All values are given in degrees.

nucleotide	RNA	HYB
G4	2.5 ± 1.1	3.4 ± 7.1
C5	4.6 ± 2.7	7.8 ± 0.5
U/T6	6.1 ± 0.9	8.7 ± 4.5
A7	3.4 ± 1.0	8.0 ± 0.8
A8	9.9 ± 1.9	5.4 ± 2.3

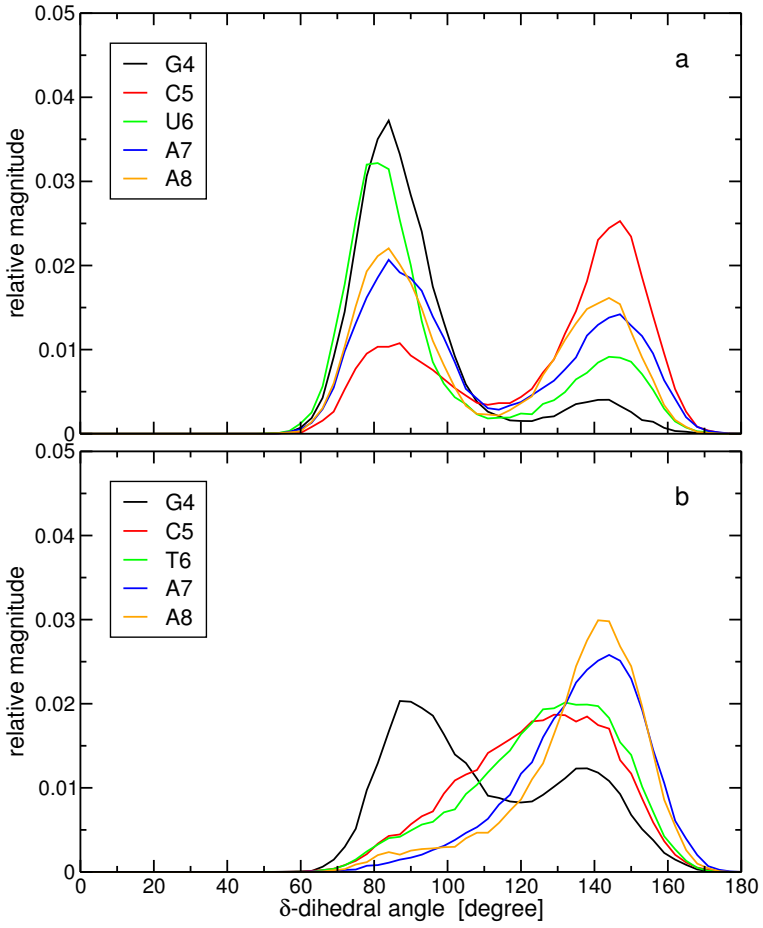

Figure S13: The normalized distribution of the δ-dihedral angle of the five nucleotides of the pentaloop for (a) the RNA and (b) the hybrid 11mer nucleotides at T=300 K.

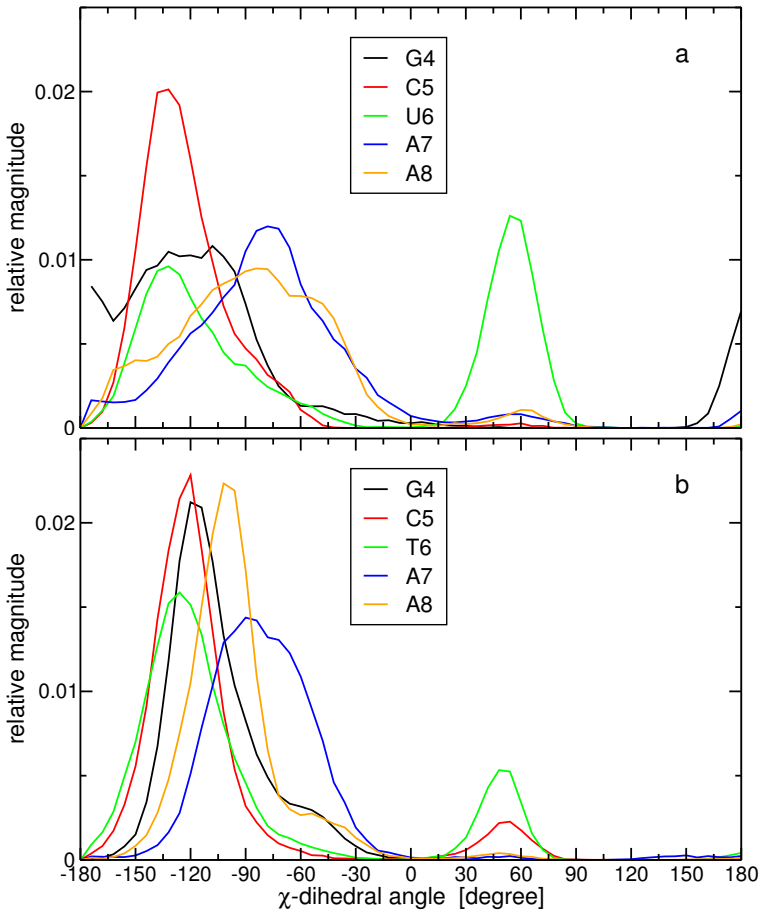

Figure S14: The normalized distribution of the χ-dihedral angle of the five nucleotides of the pentaloop for (a) the RNA and (b) the hybrid 11mer nucleotides at T=300 K.